

Quantum Synchronization of Perturbed Oscillating Coherences

Yi J. Zhao,¹ Joel E. Moore,^{1,2,3} Juzar Thingna,^{4,5,*} and Christopher W. Wächtler^{6,1,†}

¹*Department of Physics, University of California, Berkeley, California 94720, USA*

²*Challenge Institute for Quantum Computation, University of California, Berkeley, California 94720, USA.*

³*Lawrence Berkeley National Laboratory, Berkeley, CA 94720, USA*

⁴*American Physical Society, 100 Motor Parkway, Hauppauge, New York 11788, USA*

⁵*Center for Theoretical Physics of Complex Systems,
Institute for Basic Science (IBS), Daejeon 34126, Republic of Korea*

⁶*Instituto de Ciencia de Materiales de Madrid ICMN-CSIC, Madrid 28049, Spain*

(Dated: October 14, 2025)

Synchronization in quantum systems has been recently studied through persistent oscillations of local observables, which stem from undamped modes of the dissipative dynamics. However, the existence of such modes requires fine-tuning the system to satisfy specific symmetry constraints. We investigate the response of spin systems that possess such oscillating modes to generic, weak perturbations. We show that even when these perturbations break the symmetry and lead to a single steady state, the phase correlations in the resulting state exhibit signatures of synchronization. Our results therefore connect the persistent oscillation notion (*dynamical*) and the notion based on phase correlations (*steady-state*) of synchronization, which so far have been regarded as distinct phenomena. Furthermore, we demonstrate that steady-state synchronization in these systems can exhibit features that are absent in the dynamical synchronization. Our work suggests robustness of synchronization and points toward a potential unifying framework of quantum synchronization.

Introduction.—As one of the striking manifestations of collective behaviors, synchronization appears in diverse systems ranging from nearby placed pendulum clocks to organisms following circadian rhythms [1–3]. The universality of synchronization makes it a central paradigm for studying complex dynamics and bears practical implications for modern technologies [4–6]. The question whether open quantum systems can also synchronize, like their classical counterparts, has moved to the forefront of investigations in the last decade [7–17].

In the quantum regime, there have been several approaches for characterizing synchronization [7, 8, 18–27]. However, two of these characterizations are purely quantum and thus lack a classical limit. One approach is based on the time evolution of observables [19, 20, 28, 29]: The system is said to be synchronized if, at late times, the expectation values of local observables exhibit equivalent dynamics, e.g., oscillate with fixed phase differences. The other approach concerns the steady (as opposed to evolving) state: The system features synchronization if the steady state exhibits correlation (characterized by, e.g., Husimi-Q or Wigner functions) that suggests fixed phase differences either among subsystems [9, 30–35] or between the system and an external drive [8, 36–39]. Both approaches have been adopted in experimental verifications of the phenomenology [40–44].

The two notions of quantum synchronization concern distinct domains in the rich dynamical landscape of open quantum systems. The former notion, which we refer to as *dynamical synchronization*, relies on the existence of oscillating modes and has been discovered only in systems with a parameter space constrained by fine-tuning [29], symmetries [19, 20], or symmetry-protected topological order [28]. On the other hand, the latter *steady-state*

synchronization has so far only been applied to systems whose dynamics is attracted to a unique, non-oscillating steady state. This time-independent form of synchronization is not subject to strict fine-tuning and thus is distinct from that of dynamical synchronization. This distinction leads to the question whether the two *purely quantum* notions of synchronization are related or not.

In this Letter, we establish a connection between the above two notions of quantum synchronization. Our main observation is that, in dissipative systems that possess oscillating modes (a necessary condition for dynamical synchronization) [45–48], steady-state synchronization occurs in the vicinity of the fine-tuned parameter space. We explore this vicinity by introducing a set of generic perturbations, each of which leads to a single steady state that, as we show, features synchronization (see Fig. 1). Interestingly, the resulting steady-state synchronization may exhibit richer features than expected from the dynamical counterpart. Our work reveals a connection between the two notions and steps closer to a unifying theory of quantum synchronization. In the following, we start by outlining our observation under general setups, before showcasing its applicability to models possessing oscillating modes.

General setup.—To connect the two notions of quantum synchronization, we focus on dissipative dynamics in systems with a finite-dimensional Hilbert space \mathbf{H} . The reduced density matrix ϱ evolves via the Lindblad equation as $\partial_t \varrho = \mathcal{L}[\varrho]$, where

$$\mathcal{L}[\varrho] = -i[H, \varrho] + \sum_{\mu} \left(L_{\mu} \varrho L_{\mu}^{\dagger} - \frac{1}{2} \{L_{\mu}^{\dagger} L_{\mu}, \varrho\} \right), \quad (1)$$

in terms of the Hamiltonian H and the Lindblad jump

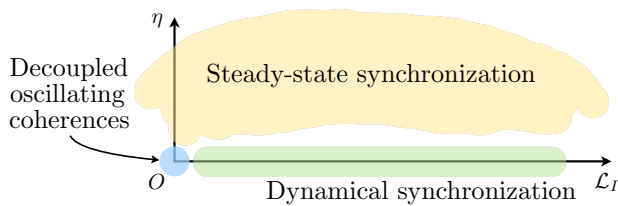


Figure 1. The two domains of synchronization. At the perturbation strength $\eta = 0$, oscillating coherences may be present either when the subsystems are decoupled ($\mathcal{L}_I = 0$) or when they are coupled through an engineered Liouvillian ($\mathcal{L}_I \neq 0$) that fulfills the criteria of dynamical synchronization (illustrated via the green region). Both cases exhibit steady-state synchronization (illustrated via the yellow region) once a generic perturbation $\eta > 0$ is introduced, breaking the fine-tuned constraints of dynamical synchronization.

operators L_μ . The Liouvillian \mathcal{L} may be viewed as a linear super-operator acting on the operator space $\mathbf{B} = \{|\psi\rangle\langle\phi| : |\psi\rangle, |\phi\rangle \in \mathbf{H}\}$. The eigenvalues λ of \mathcal{L} are complex numbers with $\text{Re}[\lambda] \leq 0$. For every right eigenmode ρ of \mathcal{L} with eigenvalue λ , the form of Eq. (1) guarantees that ρ^\dagger is an eigenmode with eigenvalue λ^* [49, 50].

Synchronization is an asymptotic behavior and thus reflected in the eigenmodes of \mathcal{L} with $\text{Re}[\lambda] = 0$. These eigenmodes span a decay-free linear subspace \mathbf{B}_{free} . Among these eigenmodes, the steady states have $\lambda = 0$, and we denote the subspace they span by \mathbf{B}_∞ . Every Liouvillian \mathcal{L} has at least one steady state [51]. The other eigenmodes in \mathbf{B}_{free} are traceless and are called *oscillating coherences*; to be precise, they span a subspace \mathbf{B}_{osc} such that $\mathbf{B}_{\text{free}} = \mathbf{B}_\infty \oplus \mathbf{B}_{\text{osc}}$. Every oscillating coherence ρ^{osc} in \mathbf{B}_{osc} has an eigenvalue $\lambda = i\omega$ for some $\omega \in \mathbb{R}$ and contributes to the time evolution of ρ a term proportional to $\rho^{\text{osc}} e^{i\omega t} + \text{H.c.}$ We emphasize that $\omega = 0$ is possible: In this case, ρ^{osc} (being traceless) is still distinguished from the steady states (with unit trace), but we call both *zero modes*. If $\omega \neq 0$, this term leads to persistent oscillation in the expectation value of any observable O satisfying $\text{Tr}[O\rho^{\text{osc}}] \neq 0$ (e.g., the Pauli operator σ^x in the spin-1/2 model [20], also discussed in App. D), under generic initial states ρ_{init} . If there are more than one such observable, O_j, O_k , supported on two different subsystems j, k , then $\langle O_j \rangle(t), \langle O_k \rangle(t)$ oscillate at the same frequency ω , with a fixed phase difference independent of the initial state. In this case, the system features dynamical synchronization [52].

The steady-state synchronization, in contrast, concerns the eigenmodes in \mathbf{B}_∞ rather than \mathbf{B}_{osc} . The synchronization under this notion is usually investigated in systems that have a unique steady state ρ^∞ and no oscillating modes. Such a system always evolves [following Eq. (1)] to ρ^∞ at late times, where synchronization occurs if the different subsystems are correlated in the sense that they are likely to differ by a fixed phase. Technically, such correlations are commonly characterized by

their joint distribution [33–35, 37]. For example, in an N -spin system the quantity of interest has been the joint distribution $S(\phi)$, where $\phi = (\phi_1, \dots, \phi_N)$ refers to the Euler angles ϕ_j (of spin j) in the plane that is perpendicular to the z -direction. We explicitly define $S(\phi)$ in terms of the Husimi- Q representation [53] based on the $\text{SU}(2)$ coherent states in App. A. As synchronization is manifested in fixed angular differences, in practice it suffices to consider the joint distribution of $\phi'_j = \phi_j - \phi_N$ ($\forall j = 1, \dots, N-1$), namely,

$$S_d(\phi') = \int_0^{2\pi} d\phi_N S(\phi'_1 + \phi_N, \dots, \phi'_{N-1} + \phi_N, \phi_N). \quad (2)$$

Its maximum, calibrated by the uniform distribution, defines the *steady-state synchronization measure*,

$$S_{\text{max}} = \max_{\phi'} S_d(\phi') - (1/2\pi)^{N-1}, \quad (3)$$

which is nonzero only if the steady-state contains off-diagonal entries in the computation basis along the z -direction. This agrees with the interpretation that limit cycles are diagonal states with $S_{\text{max}} = 0$ (see App. A).

Connecting the two notions of synchronization.—As a starting point, we consider systems whose Liouvillian \mathcal{L} has at least one oscillating coherence ρ^{osc} , a necessary condition for dynamical synchronization. A system of this sort is known to feature algebraic relations [20] among L_μ, H, ρ^∞ that imply the existence of more than one zero mode $\rho_\alpha^{\lambda=0}$, which we index by α . Under *generic perturbations*, these algebraic relations are no longer satisfied, so we expect only one steady state $\rho_{\text{pert}}^\infty$. To the leading order of the perturbation theory, we then have

$$\rho_{\text{pert}}^\infty = \sum_{\alpha} c_\alpha \rho_\alpha^{\lambda=0}, \quad (4)$$

where c_α depend on the particular form of perturbation but guarantee that $\rho_{\text{pert}}^\infty$ is a well-defined steady state [54].

Identifying steady-state synchronization in the perturbed system then involves evaluating the synchronization measure [defined in Eq. (3)] for $\rho_{\text{pert}}^\infty$. While such evaluation depends on the specific setup of the problem, for all the examples we consider below we are able to identify off-diagonal entries (in the computation basis) in at least one of the $\rho_\alpha^{\lambda=0}$. These off-diagonal entries lead to steady-state synchronization in the perturbed system.

Weakly coupled individual oscillating coherences.—In the following, we show the existence of off-diagonal entries in the perturbed steady state $\rho_{\text{pert}}^\infty$ for a special class of systems, namely those of decoupled identical spins each hosting at least one oscillating coherence (Fig. 1, blue dot). In this case, generic perturbations take the form of interactions and jump operators that weakly couple the spins. For the case where the unperturbed system itself is strongly coupled (Fig. 1, green region) we will test

our arguments with specific examples, leaving a potential general theory for future works.

We focus on $N = 2$ for brevity, as similar analysis carries over to $N > 2$. Consider a single spin governed by a Liouvillian \mathcal{L} possessing two oscillating coherences ρ^{osc} , $(\rho^{\text{osc}})^\dagger$ with eigenvalues $\pm i\omega$, respectively, and steady states ρ_α^∞ . Now consider two copies of the same system, labeled by $j = 1, 2$; to be precise, for all α, j we now have $\mathcal{L}_j[\rho_j^{\text{osc}}] = i\omega\rho_j^{\text{osc}}$, $\mathcal{L}_j[(\rho_j^{\text{osc}})^\dagger] = -i\omega(\rho_j^{\text{osc}})^\dagger$, and $\mathcal{L}_j[\rho_{\alpha,j}^\infty] = 0$.

Importantly, before any couplings between the two sites are introduced, the zero modes of the entire system include not only the steady states $\rho_{\alpha,1}^\infty \otimes \rho_{\alpha',2}^\infty$ but also the oscillating coherences $\rho_{\lambda=0}^{\text{osc}} = \rho_1^{\text{osc}} \otimes (\rho_2^{\text{osc}})^\dagger$ and $(\rho_{\lambda=0}^{\text{osc}})^\dagger$. Indeed, for example, $(\mathcal{L}_1 + \mathcal{L}_2)[\rho_{\lambda=0}^{\text{osc}}] = 0$ and $\text{Tr}[\rho_1^{\text{osc}} \otimes (\rho_2^{\text{osc}})^\dagger] = 0$ since the individual oscillating coherences have zero trace. There are additional oscillating coherences $\rho_{\lambda=2i\omega}^{\text{osc}} = \rho_1^{\text{osc}} \otimes \rho_2^{\text{osc}}$ and $(\rho_{\lambda=2i\omega}^{\text{osc}})^\dagger$, with eigenvalues $\pm 2i\omega$, respectively.

In reality, the system is subject to some perturbations, e.g., weak interactions between the two spins, and we can view the Liouvillian of the entire system as perturbed from $\mathcal{L}_1 + \mathcal{L}_2$. Generically, the perturbed system is left with one steady state, of the form described in Eq. (4),

$$\rho_{\text{pert}}^\infty = (c_{\lambda=0}\rho_{\lambda=0}^{\text{osc}} + \text{H.c.}) + \sum_{\alpha,\alpha'} c_{\alpha,\alpha'} \rho_{\alpha,1}^\infty \otimes \rho_{\alpha',2}^\infty, \quad (5)$$

for some real numbers $c_{\alpha,\alpha'}$ and a complex number $c_{\lambda=0}$. The first term in $\rho_{\text{pert}}^\infty$ is traceless and thus contributes off-diagonal entries. These off-diagonal entries in the steady state typically contribute to the steady-state synchronization measure defined in Eq. (3) and thus signals steady-state synchronization. We examine in App. E an established two-spin model of steady-state synchronization [33] and show that the model can serve as a concrete example featuring the mechanism we have described.

Spin-1 model.—While the previous case, which encompasses a broad class of models, allows us to make the connection rigorous, here we investigate a specific example [19] to demonstrate that the connection we propose also holds in the case of a strongly coupled model. The Hamiltonian of spin-1s reads

$$H = \omega \sum_j S_j^z + \sum_{j=1}^{N-1} J (S_j^+ S_{j+1}^- + \text{H.c.}) + \Delta \sum_{j=1}^{N-1} S_j^z S_{j+1}^z, \quad (6)$$

with the jump operators $L_j = \sqrt{\gamma} (S_j^z)^2$ acting on every spin $j = 1, \dots, N$. Here, the raising and lowering operators on a spin j are given by $S_j^\pm |m\rangle_j = \sqrt{S(S+1) - m(m \pm 1)} |m \pm 1\rangle_j$ with $S = 1$ and magnetization in the z -direction $m = -1, 0, 1$. These operators define $S_j^{x,y}$ through $S_j^\pm = S_j^x \pm iS_j^y$, and $S^z |m\rangle_j = m |m\rangle_j$.

The model has a strong symmetry [55] that facilitates analytical analysis, generated by the total magnetization

$M = \sum_j S_j^z$ with eigenvalues $-N, \dots, -1, 0, 1, \dots, N$. The $M = 0$ sector is further split by a strong \mathbb{Z}_2 symmetry, $P = \bigotimes_j (|1\rangle_j \langle -1|_j + |0\rangle_j \langle 0|_j + |-1\rangle_j \langle 1|_j)$ of global spin flip. We denote the two sectors corresponding to the eigenvalues $P = \pm 1$ by $0\pm$, respectively. We therefore expect $2(N+1)$ linearly independent steady states. In particular, as the unperturbed system has only Hermitian jump operators, we identify $\rho_\alpha^\infty = \mathbf{1}_\alpha$ as the maximally mixed state for every sector labeled by $\alpha = 0\pm, \pm 1, \dots, \pm N$ (see App. B for details).

The oscillating coherences arise from the resonating oscillation between the $\pm M$ sectors for $M \neq 0$ [19]. Specifically, in terms of the steady states $\rho_M^\infty = \mathbf{1}_M$ we have $\rho_M^{\text{osc}} = P\mathbf{1}_M$. Indeed, one can verify $\mathcal{L}[\rho_M^{\text{osc}}] = 2i\omega\rho_M^{\text{osc}}$, noting especially $[L_j, \rho_M^{\text{osc}}] = [L_j^\dagger, \rho_M^{\text{osc}}] = 0$ for all j and $[P, H] = \omega[P, M] = 2\omega M$. Consequently, a single-site observable O_j whose expectation value features persistent oscillation must hybridize the $| -1\rangle_j \otimes |0 \dots 0\rangle, |1\rangle_j \otimes |0 \dots 0\rangle$ states, and in particular $\text{Tr}[O_j \rho_M^{\text{osc}}] \neq 0$ if and only if $M = \pm 1$. One such observable is $O_j = (S_j^x)^2$, which is known [19] to feature dynamical synchronization at frequency 2ω .

We now consider generic perturbations. Following Eq. (4), the steady state is a mixture of the unperturbed ones, $\rho_{\text{pert}}^\infty = \sum_\alpha c_\alpha \mathbf{1}_\alpha$, for some real numbers $c_\alpha \geq 0$ satisfying $\sum_\alpha c_\alpha = 1$. To compute the steady-state synchronization measure S_{max} [see Eq. (3)], we note that $\mathbf{1}_\alpha$ contains off-diagonal entries in the computation basis only if $\alpha = 0\pm$. We list them explicitly for $N = 3$,

$$\rho_{\text{pert}}^\infty - \text{diag}[\rho_{\text{pert}}^\infty] = \frac{c_{0+} - c_{0-}}{2} (|1, -1, 0\rangle \langle -1, 1, 0| + |0, 1, -1\rangle \langle 0, -1, 1| + |-1, 0, 1\rangle \langle 1, 0, -1| + \text{H.c.}). \quad (7)$$

Although we expect our analysis to extend to larger N , we now focus on this analytically tractable case. The resulting joint distribution of angles is

$$S(\phi) = \frac{c_{0+} - c_{0-}}{32} (\cos[2(\phi_1 - \phi_2)] + \cos[2(\phi_2 - \phi_3)] + \cos[2(\phi_3 - \phi_1)]). \quad (8)$$

Since $S(\phi)$ is invariant under global shifts, we have $S_d(\phi'_1, \phi'_2) = 2\pi S(\phi'_1, \phi'_2, 0)$ based on Eq. (2).

Intriguingly, the configurations that maximize S_d depend on the sign of $c_{0+} - c_{0-}$. In the following, we denote the relative differences among N angles by unordered N -tuples, up to permutations and global shifts modulo 2π . For example, under this notation $(0, 0, \pi)$ represents the three angles valued at $\phi, \phi, \phi + \pi$ modulo 2π at an arbitrary constant shift by ϕ . Note particularly that setting $\phi = \pi$ would give $\pi, \pi, 2\pi \equiv 0$, so $(0, 0, \pi)$ and $(0, \pi, \pi)$ are equivalent notations. If $c_{0+} > c_{0-}$, then S_d is maximized when each cosine function in Eq. (8) is maximized, i.e., when the spins are in $(0, 0, 0)$ and $(0, 0, \pi)$ configurations, which we mark with yellow symbols in Fig. 2a

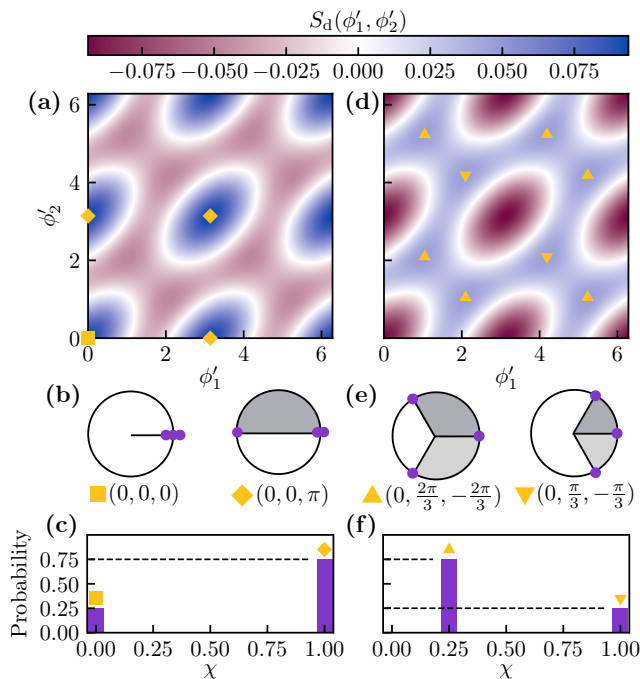


Figure 2. **(a), (d)** Distribution $S_d(\phi'_1, \phi'_2)$ [see below Eq. (8)] of the angular differences $\phi'_1 = \phi_1 - \phi_3$, $\phi'_2 = \phi_2 - \phi_3$ for the spin-1 model with $N = 3$. The distributions are for a single randomly picked sample at weak perturbation strengths $\eta \ll \omega$. Panel **(a)** corresponds to $c_{0+} > c_{0-}$ while **(d)** represents $c_{0+} < c_{0-}$. **(b), (e)** represent the angular configurations of the three spins that maximize S_d . The maxima are marked in the panels **(a)** and **(d)** with yellow symbols, each type of which corresponds to an angular configuration drawn in the panels **(b)** and **(e)** below. **(c), (f)** represent the probability of occurrence of χ for $c_{0+} > c_{0-}$ and $c_{0+} < c_{0-}$, respectively.

and represent on circle in Fig. 2b. That the angles differ by either 0 or π agrees with the dynamical synchronization of the $(S^x)^2$ operator [56]. If $c_{0-} < c_{0+}$, however, a frustration among the three cosine functions in Eq. (8) occurs, and $S(\phi)$ obtains maxima at $(0, \pi/3, -\pi/3)$ and $(0, 2\pi/3, -2\pi/3)$, marked in Fig. 2b and represented in Fig. 2e. Here, synchronization occurs with angular differences that are multiples of $\pi/3$. Remarkably, this phenomenon of $\pi/3$ -synchronization in the steady state, as opposed to the prior case of $(0, \pi)$ -synchronization, is unseen in the dynamical notion.

We numerically test the above predictions for generic perturbations at varying strengths η . As is detailed in App. F, we sample unit perturbations $\mathcal{L}_{(1)}$ from an ensemble of random Liouvillians [57] and investigate $\mathcal{L} + \eta\mathcal{L}_{(1)}$. For every realization of randomness, we have found as expected a single steady state and computed its distribution of angular differences $S_d(\phi'_1, \phi'_2)$ following Eq. (2). To examine the maxima of S_d , we characterize

angular configurations by

$$\chi(\phi_1, \phi_2, \phi_3) = \min_{j \in \{0,1,2\}} \left[\frac{3}{4\pi} \sum_i \text{argdist}(\phi_i, \bar{\phi}_j) \right]^2, \quad (9)$$

where $\bar{\phi}_j = (2\pi j + \sum_k \phi_k)/3$ are the average angles, up to $2\pi/3$ shifts that nevertheless do not affect the definition of χ . Here, $\text{argdist}(\theta, \psi) = \min_{n \in \mathbb{Z}} |\theta - \psi + 2\pi n|$ defines an angular distance on a circle. As desired, χ is invariant under global phase shifts and has values uniformly distributed in the interval $[0, 1]$ given uniformly i.i.d. angles ϕ_i (see App. C for details). We then sample $\chi(\phi'_1, \phi'_2, 0)$ based on the distribution $S_d(\phi'_1, \phi'_2)$ from those values such that S_d achieves values higher than a threshold rS_{\max} , with $r = 0.95$. We have chosen $r < 1$ to avoid potential numerical artifacts of locating more than one local maxima of similar value in $S_d(\phi'_1, \phi'_2)$.

We expect the distribution of χ sampled above to contain information on the occurrence rates of the $(0, \pi)$ - and $\pi/3$ -synchronization. Every realization of randomness of the $(0, \pi)$ type (see Fig. 2a) contributes a distribution plotted in Fig. 2c, and of the $\pi/3$ type (see Fig. 2d) plotted in Fig. 2f. These distributions reflect the situation at $r = 1$, whereas at $r < 1$ the peaks smear out. For the combined distribution of χ across all realizations of randomness, we expect smeared-out peaks around $\chi = 0, 1/4, 1$ (as seen by combining Figs. 2c, 2f). Moreover, $P(1/4)/[3P(0)]$ gives us the ratio of $\pi/3$ - to $(0, \pi)$ -synchronization. Here, $P(x)$ stands for the probability of the peak at $\chi = x$.

In Fig. 3a, for every η investigated we show the distribution of χ averaged over the ensemble of random perturbations $\mathcal{L}_{(1)}$. For $\eta/\omega \ll 1$, we identify peaks at the expected χ values (cf. Figs. 2c, 2f), indicating coexistence of $(0, \pi)$ - and $\pi/3$ -type synchronization. Strikingly, this feature persists at finite perturbation strengths up to $\eta/\omega \lesssim 10^{-3}$, suggesting robust steady-state synchronization in a finite vicinity of the $\eta = 0$ point of dynamical synchronization. As η grows further, for $\eta/\omega \gtrsim 10^{-3}$, the peaks spread out to eventually a uniform distribution of χ , suggesting uniformly distributed angles and therefore no synchronization.

Similar to the probabilities $P(x)$ (evaluated for $r = 1$) described above, we calculate the probability P_a (for $r < 1$) for the sampled χ to fall in an interval \mathcal{I}_a , $a = 1, 2, 3$, surrounding each peak. We choose the intervals to be $\mathcal{I}_1 = [0, 2/16]$, $\mathcal{I}_2 = [3/16, 5/16]$, and $\mathcal{I}_3 = [14/16, 16/16]$ to have the same length and enclose the peaks, respectively. The results are shown in Fig. 3b. The convergence of the three probabilities at $\eta/\omega \gtrsim 1$ further supports uniform distribution of χ , and thus no synchronization. In the synchronization regime $\eta/\omega \lesssim 10^{-3}$, the occurrence ratio of the $\pi/3$ - to $(0, \pi)$ -synchronization is expected to equal $P_2/(3P_1)$, which is plotted in Fig. 3c. Here, we observe that the $(0, \pi)$ - and $\pi/3$ -types of steady-state synchronization are equally likely to happen under

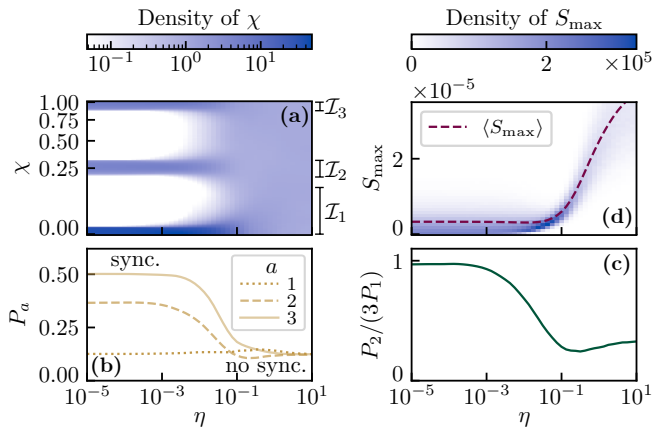


Figure 3. **(a)** Average distribution of χ as sampled from $S_d(\phi'_1, \phi'_2)$ above $0.95 \max S_d$, at varying perturbation strengths η . At $\eta \ll \omega$, the distribution shows three distinct peaks at the χ values of the spin angle configurations illustrated in Fig. 2. **(b)** The probability P_a that χ falls within the three same-sized intervals \mathcal{I}_a , $a = 1, 2, 3$, that surround the three peaks, respectively, in the $\eta \ll \omega$ limit. **(c)** The ratio $P_2/(3P_3)$, which in the $\eta \ll \omega$ limit equals the ratio of $\pi/3$ - to $(0, \pi)$ -type of synchronization. **(d)** The distribution and average of the steady-state synchronization measure S_{\max} defined in Eq. (3). We randomize over 10^4 samples and choose $\omega = 1$, $J = \Delta = 0.5$, and $\gamma = 2$.

generic, weak yet finite perturbations.

We further quantify steady-state synchronization by its measure S_{\max} as defined in Eq. (3). In Fig. 3d, we plot the distribution and average of S_{\max} across the ensemble of randomness. In the finite $\eta/\omega \lesssim 10^{-3}$ regime of synchronization, we identify an abundance of nonzero S_{\max} and furthermore nonzero $\langle S_{\max} \rangle$. This observation corroborates our above arguments, based on distributions of angular configurations, for the robustness of steady-state synchronization under generic perturbations. We emphasize that the increase of $\langle S_{\max} \rangle$ at $\eta/\omega \gtrsim 10^{-3}$, however, does not imply stronger synchronization since the angular differences are no longer locked in this regime.

In App. D, we discuss a two spin-1/2 system that hosts dynamical synchronization [20]. There, after perturbations we always observe steady-state synchronization with π -difference, coinciding with the phenomenology under the dynamical notion.

Conclusion.—We have established a direct connection between two previously independent notions of quantum synchronization: dynamical synchronization, defined through oscillating observables, and steady-state synchronization, characterized by correlations in the stationary state. Our analysis is not only a first step toward a general theory of quantum synchronization, but also shows that combining both perspectives reveals richer synchronization phenomena than either approach alone.

Acknowledgements—Y.J.Z. and J.E.M. acknowledge support from the National Science Foundation, Chal-

lenge Institute for Quantum Computation at UC Berkeley. C.W.W. was supported by the Deutsche Forschungsgemeinschaft (DFG, German Research Foundation), Project No. 496502542 (WA 5170/1-1) and received funding from the European Union’s Horizon Europe research and innovation programme under the Marie Skłodowska-Curie Actions (MSCA) grant agreement No. 101149948. This research used the Lawrence computational cluster resource provided by the IT Division at the Lawrence Berkeley National Laboratory (supported by the Director, Office of Science, Office of Basic Energy Sciences, of the U.S. Department of Energy under Contract No. DE-AC02-05CH11231).

Appendix A: The synchronization measure

In this appendix, we define the distribution $S(\phi)$ of in-plane spin angles $\phi = (\phi_1, \dots, \phi_N)$ that leads to the synchronization measure S_{\max} [given in the main text in Eq. (3)] of a steady state ρ^∞ . We then show that $S_{\max} = 0$ if ρ^∞ is diagonal in the computation basis. We remark that, rigorously, the distributions of concern in this appendix are joint quasi-probability distributions because of the quantum nature of the steady state ρ^∞ , but we nevertheless call them *distributions* for brevity.

The distribution $S(\phi)$ can be derived from the distribution $Q(\phi, \theta)$ of spin Euler angles $(\phi, \theta) = (\phi_1, \dots, \phi_N, \theta_1, \dots, \theta_N)$. The latter is known as the Husimi- Q representation of the phase space [53],

$$Q(\phi, \theta) = \langle \phi, \theta | \rho^\infty | \phi, \theta \rangle, \quad (\text{A1})$$

defined in terms of the SU(2) spin coherent states [58]

$$|\phi, \theta\rangle = \bigotimes_j \left(e^{-i\phi_j S_j^z} e^{-i\theta_j S_j^y} |S_j\rangle \right). \quad (\text{A2})$$

Here, for every spin j , we denote the local spin operators by S_j^z, S_j^y and the local state with the maximum positive magnetization by $|S_j\rangle$. As long as the synchronization of in-plane angles are concerned [33, 37], the population angles θ are irrelevant and thus integrated out. We then arrive at the distribution of the angles ϕ_j ,

$$S(\phi) = \prod_j \left(\int_0^\pi \sin \theta_j d\theta_j \right) Q(\phi, \theta), \quad (\text{A3})$$

which eventually leads to the steady-state synchronization measure through Eqs. (2) and (3), as we have elaborated in the main text.

Now we show that $S_{\max} = 0$ for diagonal ρ^∞ . Every diagonal entry contributes to ρ^∞ a component proportional to $\rho_{\mathbf{m}, \mathbf{m}} = |m_1 \dots m_N\rangle \langle m_1 \dots m_N|$, where $\mathbf{m} = (m_1, \dots, m_N)$ and m_j denotes the magnetization of the spin j , along the z direction. Note that $e^{i\phi_k S_k^z} \rho_{\mathbf{m}, \mathbf{m}} e^{-i\phi_k S_k^z}$ does not have any ϕ_k dependence,

and this holds for all k . Consequently, $Q(\phi, \theta)$ and thus $S(\phi)$ do not depend on ϕ . Since $S(\phi)$ as a distribution normalizes to unity, namely $(\prod_j \int_0^{2\pi} d\phi_j) S(\phi) = 1$, we have $S(\phi) = (1/2\pi)^N$. It therefore follows from Eqs. (2) and (3) in the main text that $S_{\max} = 0$.

Appendix B: The strong symmetry and steady states

In this appendix, we show several properties of the spin-1 model [whose Hamiltonian H and jump operators L_j are defined in Eq. (6) and below] that are mentioned in the main text. We begin by reviewing the definition of strong symmetry and its implication on the number of linearly independent steady states. We further comment on the steady states of systems whose jump operators are Hermitian.

In general, a *strong symmetry* is generated by a unitary operator that commutes with the Hamiltonian, all the jump operators, and their Hermitian conjugates [55]. As a result, the quantum numbers α of the symmetry divide the Hilbert space of the Hamiltonian into sectors $\mathbf{H} = \bigoplus_{\alpha} \mathbf{H}_{\alpha}$: The Hamiltonian and the jump operators then take block-diagonal structures in accordance with this direct sum. Consequently, every operator in $\mathbf{B}_{\alpha, \beta} = \{|\psi\rangle\langle\phi| : |\psi\rangle \in \mathbf{H}_{\alpha}, |\phi\rangle \in \mathbf{H}_{\beta}\}$ remains in the same subspace as the system evolves.

For every α , we then consider an initial state $\varrho_{\text{init}}^{\alpha} \in \mathbf{B}_{\alpha, \alpha}$ of the system: The state $\varrho_{\text{init}}^{\alpha}$ evolves to some steady state in $\mathbf{B}_{\alpha, \alpha}$. (Note however that there is no valid initial state in $\mathbf{B}_{\alpha, \beta}$ for $\alpha \neq \beta$ as every operator in this subspace is traceless.) Consequently, as has been pointed out in Ref. [55], the number of distinct α is the minimal possible number of linearly independent steady states of the system. Specifically, the spin-1 model discussed in the main text has a strong symmetry generated by the total magnetization M and the global spin flip P that leads to the quantum numbers $-N, \dots, -1, 0+, 0-, 1, \dots, N$, so we expect at least $2(N+1)$ steady states.

Additionally, for models such as this one whose jump operators are all Hermitian [i.e., $L_j = \sqrt{\gamma} (S_j^z)^2$], in every subspace $\mathbf{B}_{\alpha, \alpha}$ we can construct a steady state: the maximally mixed state $\mathbf{1}_{\alpha} = (\sum_{a=1}^{d_{\alpha}} |\psi_a\rangle\langle\psi_a|) / D_{\alpha}$. Here, $D_{\alpha} = \dim \mathbf{H}_{\alpha}$ is the dimension of the sector \mathbf{H}_{α} , for which $\{|\psi_a\rangle\}$ is an orthonormal basis. Indeed, the state $\mathbf{1}_{\alpha}$ is proportional to the identity operator of the α sector, and recall that the jump operators are block-diagonalized. One can therefore verify directly from Eq. (1) that $\mathcal{L}[\mathbf{1}_{\alpha}] = 0$.

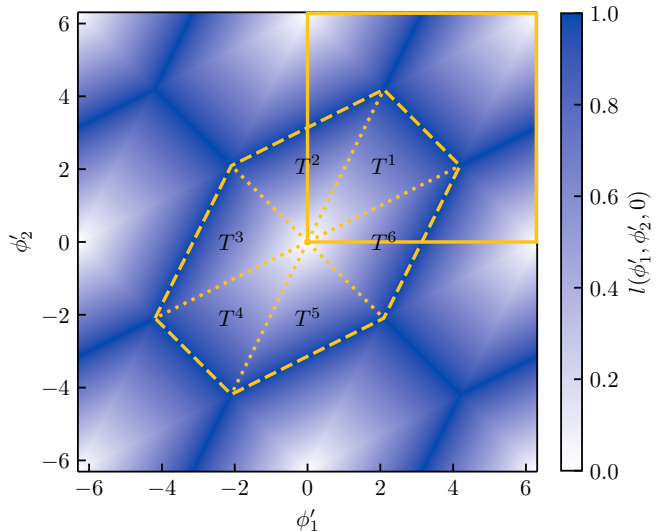


Figure 4. The $l = \sqrt{\chi}$ values of the angular differences ϕ'_1, ϕ'_2 , each ranging from -2π to 2π . The region Ω_d at $d = 1$ is enclosed in dashed lines and has an area equal to (as can be seen by shifting ϕ'_1 or ϕ'_2 by 2π) that of the square $[0, 2\pi] \times [0, 2\pi]$, enclosed by the yellow solid lines. The dotted lines illustrate, at $d = 1$, the separation of the region Ω_d into the triangles T^a .

Appendix C: The characterization function χ of angular differences

In this appendix, we comment on and derive the properties of the function $\chi(\phi_1, \phi_2, \phi_3)$, which we have defined in Eq. (9) to characterize the configurations of three angles. The χ function can be expressed as $\chi = l^2$ in terms of

$$l(\phi_1, \phi_2, \phi_3) = \frac{3}{4\pi} \min_{j \in \{0,1,2\}} \sum_i \text{argdist}(\phi_i, \bar{\phi}_j), \quad (\text{C1})$$

which is a sum of the angular distances [on a circle, defined accompanying Eq. (9)] from each angle to an optimal (in the sense that the sum is minimized) average angle $\bar{\phi}_j = (2\pi j + \sum_k \phi_k) / 3$. We always equate $\phi \equiv \phi + 2\pi n$ for every angle ϕ and integer n , so the average angle is defined up to $2\pi/3$. While equivalent representatives of the angles ϕ_1, ϕ_2, ϕ_3 may affect $\bar{\phi}_j$ for a specific j , the set $\{\bar{\phi}_j\}_{j=0,1,2}$ is invariant. The function l and thus χ are therefore well-defined functions of the three angles.

We further note that χ, l are invariant under global phase shifts mapping $\phi_j \mapsto \phi_j + \theta \forall j$ by a constant θ ; indeed, these shifts also map the average angles in the way $\bar{\phi}_k \mapsto \bar{\phi}_k + \theta \forall k$, so the angular distances, $\text{argdist}(\phi_j, \bar{\phi}_k)$, are unchanged. Therefore, χ, l are sensitive to only the differences among the angles ϕ_i and thus suitable for characterizing synchronization. In particular, $\chi(\phi_1, \phi_2, \phi_3) = \chi(\phi'_1, \phi'_2, 0)$ and $l(\phi_1, \phi_2, \phi_3) = l(\phi'_1, \phi'_2, 0)$ in terms of the differences $\phi'_j = \phi_j - \phi_3$, for

$j = 1, 2$, defined in the main text.

The χ function bears another useful property, namely that $\chi(\phi_1, \phi_2, \phi_3)$ is uniformly distributed in $[0, 1]$ if the angles ϕ_1, ϕ_2, ϕ_3 are uniformly i.i.d. In the main text, we have used this property to argue for a non-synchronization regime. To show this property, it suffices to show that $l(\phi'_1, \phi'_2)$, which we use to denote $l(\phi'_1, \phi'_2, 0) = \sqrt{\chi(\phi'_1, \phi'_2, 0)}$, takes values in $[0, 1]$ and follows the distribution $f(l) = 2l$ given uniformly i.i.d. ϕ_1, ϕ_2, ϕ_3 , i.e., uniformly i.i.d. angular differences ϕ'_1, ϕ'_2 .

We start by considering the cumulative distribution $F(l) = \int_0^l f(l')dl'$. We claim that, given $d \in (0, 1]$, the following region $\Omega_d \subset \{(\phi'_1, \phi'_2) : \phi'_1, \phi'_2 \in [-2\pi, 2\pi]\}$ given by $\Omega_d = \bigcup_{a=1}^6 \overline{T_d^a}$ satisfies $l(\Omega_d) < d$ and $l(\partial\Omega_d) = d$, where T_d^a are disjoint triangles,

$$\begin{aligned} T_d^1 &= \{0 < \phi'_1 + \phi'_2 < 2\pi d, \phi'_1 - 2\phi'_2 < 0, 2\phi'_1 - \phi'_2 > 0\} \\ T_d^2 &= \{0 < 2\phi'_2 - \phi'_1 < 2\pi d, 2\phi'_1 - \phi'_2 < 0, \phi'_1 + \phi'_2 > 0\} \\ T_d^3 &= \{0 < \phi'_2 - \phi'_1 < 2\pi d, \phi'_1 + \phi'_2 < 0, \phi'_1 - 2\phi'_2 < 0\}, \\ T_d^4 &= -T_d^1, \quad T_d^5 = -T_d^2, \quad T_d^6 = -T_d^3, \end{aligned} \quad (\text{C2})$$

and $\overline{T_d^a}$ denotes the closure of T_d^a ; we draw T_d^a at $d = 1$ in Fig. 4. Indeed, one can check for every ϕ'_1, ϕ'_2 in, e.g., T_d^1 that the average angle $\bar{\phi}_j = (2\pi j + \phi'_1 + \phi'_2)/3$ achieving $l(\phi'_1, \phi'_2, 0)$ in Eq. (C1) has $j = 0$, that

$$\begin{aligned} \text{argdist}(\phi'_1, \bar{\phi}_0) &= \frac{2\phi'_1 - \phi'_2}{3} \\ \text{argdist}(\phi'_2, \bar{\phi}_0) &= \frac{2\phi'_2 - \phi'_1}{3} \\ \text{argdist}(0, \bar{\phi}_0) &= \frac{\phi'_1 + \phi'_2}{3}, \end{aligned} \quad (\text{C3})$$

and therefore that $l(\phi'_1, \phi'_2) = (\phi'_1 + \phi'_2)/2\pi < d$. Moreover, $(\phi'_1, \phi'_2) \in \partial T_d^1$ is in $\partial\Omega_d$ if and only if $\phi'_1 + \phi'_2 = 2\pi d$, so we can conclude for such ϕ'_1, ϕ'_2 that $l(\phi'_1, \phi'_2) = d$. In general, for every T_d^a listed above we can specify the average angle $\bar{\phi}_j$ that is relevant for computing l and thus straightforwardly verify the similar properties.

We then conclude based on Eq. (C2) and similar equations for all the six triangles T_d^a that the area of Ω_d is proportional to d^2 . We furthermore specify this area to be $(2\pi d)^2$ by noting that the area at $d = 1$ equals that of a square of length 2π (cf. Fig. 4). Since the latter square already contains all the equivalent values of ϕ'_1, ϕ'_2 , we see that l takes values from $[0, 1]$. Additionally following from the area calculation, for uniformly i.i.d. ϕ'_1, ϕ'_2 we have the cumulative distribution $F(l) = (2\pi l)^2 / (2\pi)^2 = l^2$ and thus the distribution $f(l) = dF(l)/dl = 2l$ as desired.

Appendix D: A spin-1/2 model of dynamical synchronization

We consider a system of two spin-1/2s that is simplified from the one reported to feature dynamical syn-

chronization in Ref. [20]. The system is governed by the Hamiltonian

$$H = J(\sigma_1^+ \sigma_2^- + \text{H.c.}) + \Delta \sigma_1^z \sigma_2^z + B(\sigma_1^z + \sigma_2^z), \quad (\text{D1})$$

and jump operators

$$L_- = \gamma(\sigma_1^- + \sigma_2^-). \quad (\text{D2})$$

Here, $\sigma_j^\pm = (\sigma_j^x \pm i\sigma_j^y)/2$ in terms of the Pauli operators acting on the spins $j = 1, 2$.

We note a strong inversion symmetry P that is helpful for analyzing the system, given by

$$P = |\uparrow\uparrow\rangle\langle\downarrow\downarrow| + |\downarrow\downarrow\rangle\langle\uparrow\uparrow| + |\uparrow\downarrow\rangle\langle\downarrow\uparrow| + |\downarrow\uparrow\rangle\langle\uparrow\downarrow|, \quad (\text{D3})$$

with eigenvalues $P = \pm 1$. The operator P generates a strong symmetry [55] because it satisfies $[H, P] = [P, L_-] = 0$. It therefore preserves the dynamics within every Hilbert space corresponding to one of the eigenvalues,

$$\begin{aligned} \mathbf{H}_+ &= \text{span} \left\{ |\uparrow\uparrow\rangle, \frac{1}{\sqrt{2}}(|\uparrow\downarrow\rangle + |\downarrow\uparrow\rangle), |v_+\rangle = |\downarrow\downarrow\rangle \right\} \\ \mathbf{H}_- &= \text{span} \left\{ |v_-\rangle = \frac{1}{\sqrt{2}}(|\uparrow\downarrow\rangle - |\downarrow\uparrow\rangle) \right\}. \end{aligned} \quad (\text{D4})$$

Here, the states $|v_\pm\rangle$ we have defined are in fact the dark states, as each of $|v_+\rangle\langle v_+|, |v_-\rangle\langle v_-|$ is the steady states of the $\mathbf{B}_{++}, \mathbf{B}_{--}$ operator subspaces, respectively; note that $|v_\pm\rangle$ are eigenstates of H with energies $\Delta - 2B, -2J - \Delta$, and that $L_- |v_+\rangle = L_- |v_-\rangle = 0$. We elaborate on the properties of the strong symmetry and define the relevant notations in App. B to the main text.

Following the above analysis, the system possesses an oscillating coherence $\rho^{\text{osc}} = |v_+\rangle\langle v_-|$ at frequency $\omega = 2(J - \Delta + B)$. Every observable O whose expectation value features the dynamical synchronization satisfies $\text{Tr}[O\rho^{\text{osc}}] \neq 0$. Single-site observables of this sort include σ_j^x, σ_j^y , for $j = 1, 2$. For instance, $\langle\sigma_1^x(t)\rangle$ synchronizes with $-\langle\sigma_2^x(t)\rangle$. The negative sign here indicates that the two spins are synchronized with fixed phase difference π .

We now consider perturbations that explicitly break the strong symmetry P and result in a single steady state $\rho_{\text{pert}}^\infty$. For the generic case where perturbations in both the Hamiltonian H and the jump operators are present, we expect from Eq. (4) that $\rho_{\text{pert}}^\infty = c_+ |v_+\rangle\langle v_+| + c_- |v_-\rangle\langle v_-|$, with $c_\pm \geq 0$ satisfying $c_+ + c_- = 1$ for unit trace. To evaluate the steady-state synchronization measure S_{max} defined in Eq. (3), note that $|v_+\rangle\langle v_+|$ does not contribute to S_{max} as it contains no off-diagonal entries in the computation basis. The only contribution comes from the $c_- |v_-\rangle\langle v_-|$ term, so the joint distribution of the in-plane angles ϕ_1, ϕ_2 reads (see also App. A to the main text)

$$S(\phi_1, \phi_2) = -c_- \cos(\phi_1 - \phi_2). \quad (\text{D5})$$

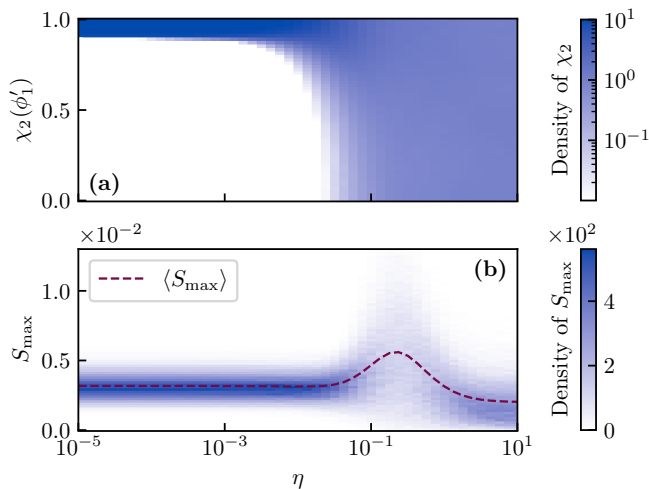


Figure 5. The model of two spin-1/2s [described in Eqs. (D1) and (D2), with $J = 1$, $\Delta = 1$, $B = 0.3$, $\gamma = 0.5$] under generic random perturbations at strengths η . Data represent average over 10^4 realizations of randomness. (a) The distribution of $\chi_2(\phi'_1)$ characterizing the phase difference $\phi'_1 = \phi_1 - \phi_2$, sampled from angular configurations such that S_d achieves higher than $0.95S_{\max}$. (b) The distribution of S_{\max} , the measure of steady-state synchronization, and its average, $\langle S_{\max} \rangle$.

Following Eq. (2), $S_d(\phi'_1) = -2\pi c_- \cos(\phi'_1)$ in terms of the angular difference $\phi'_1 = \phi_1 - \phi_2$.

We then find that S_d achieves $S_{\max} = c_- \geq 0$ when $\phi'_1 = \pi$: The perturbed system features steady-state synchronization between the spins 1 and 2. Notably, the observation that the in-plane angles ϕ_1 , ϕ_2 most likely differ by π agrees with the dynamical notion, where the expectation values of observables σ^x , σ^y at the two spins show persistent oscillations with a sign difference, also suggesting an in-plane angular difference π .

We verify numerically that generic weak perturbations indeed lead to $S_{\max} > 0$ and, moreover, synchronization at the angular difference π . In particular, we sample unit perturbations $\mathcal{L}_{(1)}$ from an ensemble of random Liouvillian defined in Ref. [57] and study the dynamics given by $\mathcal{L} + \eta\mathcal{L}_{(1)}$ at varying strength η . We detail our sampling method in App. F. For every realization of randomness, we have found as expected a single steady state, computed its steady-state synchronization measure S_{\max} [defined in Eq. (3)], and kept track of the normalized angular difference in terms $\phi'_1 = \phi_1 - \phi_2$,

$$\chi_2(\phi'_1) = \frac{1}{\pi} \text{argdist}(\phi'_1, 0). \quad (\text{D6})$$

Here and also in the main text, we use $\text{argdist}(\theta, \psi) = \min_{n \in \mathbb{Z}} |\theta - \psi + 2\pi n|$ to define an angular distance on circle. Note that, in fashion similar to the χ function characterizing the angular differences of three angles in the main text, here χ_2 is uniformly distributed in $[0, 1]$ if the angles ϕ_1 , ϕ_2 are uniformly i.i.d.

In Fig. 5, we plot the distributions of χ_2 and S_{\max} for

increasing η . To avoid potential numerical artifacts of locating more than one local maxima of similar values, we sample $\chi_2(\phi'_1)$ from those ϕ'_1 where $S_d(\phi'_1)$ achieves above a threshold rS_{\max} , with $r = 0.95$. We find typically nonzero S_{\max} at all η we accessed, including η that are significantly smaller than the energy scale J in the unperturbed model. This suggests steady-state synchronization in a finite vicinity of the fine-tuned $\eta = 0$ point of dynamical synchronization. In addition, while we observe uniform distribution of χ indicating uniformly i.i.d. ϕ_1, ϕ_2 and thus no synchronization for $\eta/J \gtrsim 10^{-1}$, at small $\eta/J \lesssim 10^{-2}$ we find χ_2 concentrated around $\chi_2 = 1$. This suggests that ϕ_1, ϕ_2 most likely differ by π in the steady-state synchronization regime, as is expected from our perturbative analysis in Eq. (D5).

Appendix E: Steady-state synchronization of two weakly coupled spin-1's

We give a concrete example where two decoupled spins hosting oscillating coherences feature steady-state synchronization after perturbative couplings. We adopt the example from an established model of steady-state synchronization [33] and show that the results there in some regimes can be interpreted with the general arguments presented in our main text.

The original model consists of two spin-1s. To fit the model under our general arguments, we view the model as governed by the decoupled Hamiltonian and jump operators, on the two spins $j = 1, 2$,

$$H_j = \omega S_j^z \quad \forall j$$

$$L_1^g = \sqrt{\frac{\gamma_1^g}{2}} S_1^+ S_1^z, \quad L_2^d = \sqrt{\frac{\gamma_2^d}{2}} S_2^- S_2^z, \quad (\text{E1})$$

that give rise to the Liouvillians \mathcal{L}_1 , \mathcal{L}_2 , respectively, according to Eq. (1). Additionally, the Liouvillian $\mathcal{L} = \mathcal{L}_1 + \mathcal{L}_2 + \mathcal{L}_{(1)}$ of the entire system contains perturbation $\mathcal{L}_{(1)}$ contributed by

$$H_{(1)} = \frac{i\epsilon}{2} (S_1^+ S_2^- - S_1^- S_2^+) + \sum_j \Delta_j S_j^z$$

$$L_1^d = \sqrt{\frac{\gamma_1^d}{2}} S_1^- S_1^z, \quad L_2^g = \sqrt{\frac{\gamma_2^g}{2}} S_2^+ S_2^z. \quad (\text{E2})$$

We focus on the weak perturbation regime defined by $\epsilon, \Delta_1, \Delta_2, \gamma_1^d, \gamma_2^g \ll \omega, \gamma_1^g, \gamma_2^d$, where steady-state synchronization has been observed [33]. We note however that Ref. [33] has also discussed the regime of finite perturbations, especially one where $\gamma_1^d = \gamma_1^g$. This regime is out of the scope of our general arguments, which we have developed for weakly coupled oscillating coherences.

The limit of weak perturbations $\epsilon, \Delta_1, \Delta_2, \gamma_1^d, \gamma_2^g \rightarrow 0$ fits in our arguments in that the system in this limit possesses decoupled oscillating coherences

$$\rho_1^{\text{osc}} = |0\rangle_1 \langle 1|_1, \quad \rho_2^{\text{osc}} = |-1\rangle_2 \langle 0|_2, \quad (\text{E3})$$

and their Hermitian conjugates. Here, in accordance with the notation in the main text, ρ_j^{osc} denotes the oscillating coherence on the standalone spin j . Moreover, $\mathcal{L}_1[\rho_1^{\text{osc}}] = i\omega\rho_1^{\text{osc}}$, $\mathcal{L}_2[\rho_2^{\text{osc}}] = i\omega\rho_2^{\text{osc}}$, so they oscillate at the same frequency.

Under this setup, our general arguments in the main text apply. The unperturbed system therefore features (among others) the following zero modes with off-diagonal entries in the computation basis,

$$\rho_{\lambda=0}^{\text{osc}} = |0, 0\rangle\langle 1, -1|, \quad (\rho_{\lambda=0}^{\text{osc}})^\dagger. \quad (\text{E4})$$

As is argued analytically and verified numerically in Ref. [33], these entries indeed contribute to the steady-state measure S_{max} of synchronization defined in Eq. (3) in the presence of small yet nonzero $\epsilon, \Delta_1, \Delta_2, \gamma_1^d, \gamma_2^g$, which we view here as perturbative couplings.

Appendix F: Sampling generic perturbations

We elaborate on how we sample the generic random perturbations $\mathcal{L}_{(1)}$ from an ensemble of Liouvillians that is proposed in Ref. [57]. The perturbative Liouvillian $\mathcal{L}_{(1)}$ consists of two parts,

$$\mathcal{L}_{(1)}[\varrho] = i\zeta_{\text{coh}}(\varrho H_{(1)} - H_{(1)}\varrho) + \zeta_{\text{diss}}\mathcal{L}_{(1)}^{\text{diss}}[\varrho]. \quad (\text{F1})$$

Here, the first of the two terms constitutes the coherent part, evolving the system by a random Hamiltonian $H_{(1)}$ acting on a Hilbert space of dimension $D_{\mathbf{H}}$, and the second term is a purely dissipative part given by a dissipator $\mathcal{L}_{(1)}^{\text{diss}}$. Their relative contributions to the overall perturbative Liouvillian $\mathcal{L}_{(1)}$ are tuned by the real numbers $\zeta_{\text{coh}}, \zeta_{\text{diss}}$. While Ref. [57] has investigated different sets of the two parameters, for our purpose we only take $\zeta_{\text{coh}} = \zeta_{\text{diss}} = 1$; we expect this choice to represent the generic situation. We sample $H_{(1)}$ and $\mathcal{L}_{(1)}^{\text{diss}}$ independently based on the procedures described in Ref. [57], which we also summarize as follows.

We sample the Hamiltonian $H_{(1)}$ from a Gaussian unitary ensemble of unit variance. Following the standard procedure (see for example in Ref. [59]), we first sample a random $D_{\mathbf{H}}$ -by- $D_{\mathbf{H}}$ matrix M , the real and imaginary parts of whose entries are i.i.d. Gaussian random variables of mean 0 and variance 1. We then take $H_{(1)} = (M + M^\dagger)/\sqrt{2}$.

To sample the dissipator $\mathcal{L}_{(1)}^{\text{diss}}$, we start by generating a d -by- d matrix G with real and imaginary parts of the entries being i.i.d. Gaussian random variables of mean 0 and variance 1; here $d = D_{\mathbf{H}}^2 - 1$. The general form of the dissipator is then given in terms of a properly normalized matrix $K = dGG^\dagger/\text{Tr}[GG^\dagger]$,

$$\mathcal{L}_{(1)}^{\text{diss}}[\varrho] = \sum_{m,n=1}^d K_{mn} \left[F_n \varrho F_m^\dagger - \frac{1}{2} \{F_m^\dagger F_n, \varrho\} \right], \quad (\text{F2})$$

for traceless matrices F_n satisfying $\text{Tr}[F_m F_n^\dagger] = \delta_{m,n}$. In practice, we pick the $D_{\mathbf{H}}$ -by- $D_{\mathbf{H}}$ matrices F_n , where $n = 1, \dots, d$, so that their entries (indexed by j, k) are

$$(F_{(a-1)D_{\mathbf{H}}+b})_{j,k} = \begin{cases} \delta_{j,a}\delta_{k,b} & a \neq b \\ \delta_{j,a}\delta_{k,a} - \delta_{j,a+1}\delta_{k,a+1} & a = b \end{cases}, \quad (\text{F3})$$

for $a, b = 1, \dots, D_{\mathbf{H}}$ except for $a = b = D_{\mathbf{H}}$.

While Eq. (F2) is sufficient for describing our sampling approach for the perturbative dissipator $\mathcal{L}_{(1)}^{\text{diss}}$, we remark in the following that it can be written in the form as appears in a Lindblad equation [cf. Eq. (1)]. Indeed, after diagonalizing the Hermitian positive semidefinite matrix K as $K_{\sigma,\tau} = \sum_{\mu} \kappa_{\mu} V_{\mu,\sigma}^* V_{\mu,\tau}$ in terms of a d -by- d unitary matrix V and eigenvalues $\kappa_{\mu} \geq 0$, we can construct the jump operators $L_{\mu} = \sum_{\nu} \sqrt{\kappa_{\mu}} V_{\mu,\nu} F_{\nu}$ for $\mu = 1, \dots, d$. Then, Eq. (F2) is rewritten as

$$\mathcal{L}_{(1)}^{\text{diss}}[\varrho] = \sum_{\mu=1}^{D_{\mathbf{H}}^2-1} \left(L_{\mu} \varrho L_{\mu}^\dagger - \frac{1}{2} \{L_{\mu}^\dagger L_{\mu}, \varrho\} \right), \quad (\text{F4})$$

in the desired form.

* juzar18@gmail.com

† cwwaechtler@icmm.csic.es; J.T. and C.W.W. contributed equally to this work.

- [1] M. Rosenblum and A. Pikovsky, Synchronization: From pendulum clocks to chaotic lasers and chemical oscillators, *Contemporary Physics* **44**, 401 (2003).
- [2] C. A. Czeisler, J. S. Allan, S. H. Strogatz, J. M. Ronda, R. Sánchez, C. D. Ríos, W. O. Freitag, G. S. Richardson, and R. E. Kronauer, Bright light resets the human circadian pacemaker independent of the timing of the sleep-wake cycle, *Science* **233**, 667 (1986).
- [3] R. Y. Moore, A clock for the ages, *Science* **284**, 2102 (1999).
- [4] A. Pikovsky, M. Rosenblum, and J. Kurths, *Synchronization: A Universal Concept in Nonlinear Sciences*, Cambridge Nonlinear Science Series (Cambridge University Press, Cambridge, 2001).
- [5] T. Herpich, J. Thingna, and M. Esposito, Collective power: Minimal model for thermodynamics of nonequilibrium phase transitions, *Phys. Rev. X* **8**, 031056 (2018).
- [6] S. H. Strogatz, *Nonlinear Dynamics and Chaos: With Applications to Physics, Biology, Chemistry, and Engineering*, 3rd ed. (Chapman and Hall/CRC, New York, 2024).
- [7] T. E. Lee and H. R. Sadeghpour, Quantum synchronization of quantum van der Pol oscillators with trapped ions, *Phys. Rev. Lett.* **111**, 234101 (2013).
- [8] S. Walter, A. Nunnenkamp, and C. Bruder, Quantum synchronization of a driven self-sustained oscillator, *Phys. Rev. Lett.* **112**, 094102 (2014).
- [9] S. Walter, A. Nunnenkamp, and C. Bruder, Quantum synchronization of two van der Pol oscillators, *Ann. Phys.* **527**, 131 (2015).

- [10] S. Dutta and N. R. Cooper, Critical response of a quantum van der Pol oscillator, *Phys. Rev. Lett.* **123**, 250401 (2019).
- [11] N. Thomas and M. Senthilvelan, Quantum synchronization in quadratically coupled quantum van der Pol oscillators, *Phys. Rev. A* **106**, 012422 (2022).
- [12] N. Es'haqi-Sani, G. Manzano, R. Zambrini, and R. Fazio, Synchronization along quantum trajectories, *Phys. Rev. Res.* **2**, 023101 (2020).
- [13] A. Delmonte, A. Romito, G. E. Santoro, and R. Fazio, Quantum effects on the synchronization dynamics of the Kuramoto model, *Phys. Rev. A* **108**, 032219 (2023).
- [14] Y. Shen, H. Y. Soh, W. Fan, and L.-C. Kwek, Enhancing quantum synchronization through homodyne measurement and squeezing, arXiv preprint arXiv:2302.13465 (2023), arXiv:2302.13465.
- [15] F. Schmolke and E. Lutz, Measurement-induced quantum synchronization and multiplexing, arXiv preprint arXiv:2306.12986 (2023), arXiv:2306.12986.
- [16] M. Xu, D. A. Tieri, E. C. Fine, J. K. Thompson, and M. J. Holland, Synchronization of two ensembles of atoms, *Phys. Rev. Lett.* **113**, 154101 (2014).
- [17] C. W. Wächtler and G. Platero, Topological synchronization of quantum van der Pol oscillators, *Phys. Rev. Res.* **5**, 023021 (2023).
- [18] V. M. Bastidas, I. Omelchenko, A. Zakharova, E. Schöll, and T. Brandes, Quantum signatures of chimera states, *Phys. Rev. E* **92**, 062924 (2015).
- [19] J. Tindall, C. Sánchez Muñoz, B. Buča, and D. Jaksch, Quantum synchronisation enabled by dynamical symmetries and dissipation, *New J. Phys.* **22**, 013026 (2020).
- [20] B. Buča, C. Booker, and D. Jaksch, Algebraic theory of quantum synchronization and limit cycles under dissipation, *SciPost Phys.* **12**, 097 (2022).
- [21] M. Aifer, J. Thingna, and S. Deffner, Energetic cost for speedy synchronization in non-Hermitian quantum dynamics, *Phys. Rev. Lett.* **133**, 020401 (2024).
- [22] A. Mari, A. Farace, N. Didier, V. Giovannetti, and R. Fazio, Measures of quantum synchronization in continuous variable systems, *Phys. Rev. Lett.* **111**, 103605 (2013).
- [23] V. Ameri, M. Eghbali-Arani, A. Mari, A. Farace, F. Kheirandish, V. Giovannetti, and R. Fazio, Mutual information as an order parameter for quantum synchronization, *Phys. Rev. A* **91**, 012301 (2015).
- [24] N. Jaseem, M. Hajdušek, P. Solanki, L.-C. Kwek, R. Fazio, and S. Vinjanampathy, Generalized measure of quantum synchronization, *Phys. Rev. Res.* **2**, 043287 (2020).
- [25] M. Ludwig and F. Marquardt, Quantum many-body dynamics in optomechanical arrays, *Phys. Rev. Lett.* **111**, 073603 (2013).
- [26] M. R. Hush, W. Li, S. Genway, I. Lesanovsky, and A. D. Armour, Spin correlations as a probe of quantum synchronization in trapped-ion phonon lasers, *Phys. Rev. A* **91**, 061401 (2015).
- [27] T. Weiss, A. Kronwald, and F. Marquardt, Noise-induced transitions in optomechanical synchronization, *New J. Phys.* **18**, 013043 (2016).
- [28] C. W. Wächtler and J. E. Moore, Topological quantum synchronization of fractionalized spins, *Phys. Rev. Lett.* **132**, 196601 (2024).
- [29] F. Schmolke and E. Lutz, Noise-induced quantum synchronization, *Phys. Rev. Lett.* **129**, 250601 (2022).
- [30] N. Lörch, S. E. Nigg, A. Nunnenkamp, R. P. Tiwari, and C. Bruder, Quantum synchronization blockade: Energy quantization hinders synchronization of identical oscillators, *Phys. Rev. Lett.* **118**, 243602 (2017).
- [31] K. Ishibashi and R. Kanamoto, Oscillation collapse in coupled quantum van der Pol oscillators, *Phys. Rev. E* **96**, 052210 (2017).
- [32] S. Sonar, M. Hajdušek, M. Mukherjee, R. Fazio, V. Vedral, S. Vinjanampathy, and L.-C. Kwek, Squeezing enhances quantum synchronization, *Phys. Rev. Lett.* **120**, 163601 (2018).
- [33] A. Roulet and C. Bruder, Quantum synchronization and entanglement generation, *Phys. Rev. Lett.* **121**, 063601 (2018).
- [34] T. Murtadho, S. Vinjanampathy, and J. Thingna, Cooperation and competition in synchronous open quantum systems, *Phys. Rev. Lett.* **131**, 030401 (2023).
- [35] T. Murtadho, J. Thingna, and S. Vinjanampathy, Deriving lower bounds on the efficiency of near-degenerate thermal machines via synchronization, *Phys. Rev. A* **108**, 012205 (2023).
- [36] N. Lörch, E. Amitai, A. Nunnenkamp, and C. Bruder, Genuine quantum signatures in synchronization of anharmonic self-oscillators, *Phys. Rev. Lett.* **117**, 073601 (2016).
- [37] A. Roulet and C. Bruder, Synchronizing the smallest possible system, *Phys. Rev. Lett.* **121**, 053601 (2018).
- [38] W.-K. Mok, L.-C. Kwek, and H. Heimonen, Synchronization boost with single-photon dissipation in the deep quantum regime, *Phys. Rev. Res.* **2**, 033422 (2020).
- [39] W. K. Mok, L. C. Kwek, and H. Heimonen, Noise, not squeezing, boosts synchronization in the deep quantum regime, arXiv preprint arXiv:2002.07488 (2020), arXiv:2002.07488.
- [40] A. W. Laskar, P. Adhikary, S. Mondal, P. Katiyar, S. Vinjanampathy, and S. Ghosh, Observation of quantum phase synchronization in spin-1 atoms, *Phys. Rev. Lett.* **125**, 013601 (2020).
- [41] M. Koppenhöfer, C. Bruder, and A. Roulet, Quantum synchronization on the IBM Q system, *Phys. Rev. Research* **2**, 023026 (2020).
- [42] Y. Li, Z. Xie, X. Yang, Y. Li, X. Zhao, X. Cheng, X. Peng, J. Li, E. Lutz, Y. Lin, and J. Du, *Experimental realization and synchronization of a quantum van der Pol oscillator* (2025), arXiv:2504.00751 [quant-ph].
- [43] Z. Tao, F. Schmolke, C.-K. Hu, W. Huang, Y. Zhou, J. Zhang, J. Chu, L. Zhang, X. Sun, Z. Guo, J. Niu, W. Weng, S. Liu, Y. Zhong, D. Tan, D. Yu, and E. Lutz, Noise-induced quantum synchronization with entangled oscillations, *Nat Commun* **16**, 8457 (2025).
- [44] J. Liu, Q. Wu, J. E. Moore, H. Haeffner, and C. W. Wächtler, Observation of synchronization between two quantum van der Pol oscillators in trapped ions (2025), arXiv:2509.18423 [quant-ph].
- [45] V. V. Albert and L. Jiang, Symmetries and conserved quantities in Lindblad master equations, *Phys. Rev. A* **89**, 022118 (2014).
- [46] J. Thingna, D. Manzano, and J. Cao, Dynamical signatures of molecular symmetries in nonequilibrium quantum transport, *Scientific Reports* **6**, 28027 (2016).
- [47] D. Manzano and P. Hurtado, Harnessing symmetry to control quantum transport, *Advances in Physics* **67**, 1 (2018).
- [48] J. Thingna and D. Manzano, Degenerated Liouvillians

- and steady-state reduced density matrices, *Chaos: An Interdisciplinary Journal of Nonlinear Science* **31**, 073114 (2021).
- [49] G. Lindblad, On the generators of quantum dynamical semigroups, *Commun. Math. Phys.* **48**, 119 (1976).
- [50] D. Burgarth, G. Chiribella, V. Giovannetti, P. Perinotti, and K. Yuasa, Ergodic and mixing quantum channels in finite dimensions, *New J. Phys.* **15**, 073045 (2013).
- [51] D. E. Evans, Irreducible quantum dynamical semigroups, *Commun. Math. Phys.* **54**, 293 (1977).
- [52] In Ref. [60], the synchronization of multiple oscillating coherences is referred to as “coherence synchronization,” whereas in this work, in the spirit of Ref. [20], we also consider the general case of local observables being synchronized in the presence of a single pair of oscillating coherences.
- [53] K. Husimi, Some formal properties of the density matrix, *Proceedings of the Physico-Mathematical Society of Japan. 3rd Series* **22**, 264 (1940).
- [54] We emphasize that $\rho_{\text{pert}}^\infty$ is a well-defined reduced density matrix of the system and that, since $\rho_{\text{pert}}^\infty$ is the only steady state, the system always evolves to this state regardless of initial conditions.
- [55] B. Buča and T. Prosen, A note on symmetry reductions of the Lindblad equation: Transport in constrained open spin chains, *New J. Phys.* **14**, 073007 (2012).
- [56] In particular, for spins whose in-plane angles (i.e., the Euler angles in the plane perpendicular to the z -direction) differ by π or 0, we expect them to have x -components that either differ by a sign or agree. This picture agrees with the synchronization of the expectation value of $(S^x)^2$ in the dynamical notion.
- [57] S. Denisov, T. Lapyeva, W. Tarnowski, D. Chruś ński, and K. Ż Życzkowski, Universal spectra of random Lindblad operators, *Phys. Rev. Lett.* **123**, 140403 (2019).
- [58] K. Nemoto, Generalized coherent states for SU(n) systems, *Journal of Physics A: Mathematical and General* **33**, 3493 (2000).
- [59] G. W. Anderson, A. Guionnet, and O. Zeitouni, *An Introduction to Random Matrices*, Cambridge Studies in Advanced Mathematics (Cambridge University Press, 2009).
- [60] P. Solanki, N. Jaseem, M. Hajdušek, and S. Vinjanampathy, Role of coherence and degeneracies in quantum synchronization, *Phys. Rev. A* **105**, L020401 (2022).